Cyber Physical System for Data-Driven Modeling of Fused Filament Fabrication (FFF) Extrusion Process

Osama Habbal
Mechnical Engineering Department
University of Michigan Dearborn
Dearborn, USA
ohabbal@umich.edu

Maximilian Ullrich
Mechnical Engineering Department
University of Michigan Dearborn
Dearborn, USA
mullrich@umich.edu

Dawood Al Nabhani
Mechnical Engineering Department
University of Michigan Dearborn
Dearborn, USA
dalnabha@umich.edu

Pravansu Mohanty
Mechanical Engineering Department
University of Michigan Dearborn
Dearborn, USA
pmohanty@umich.edu

Zhen Hu
Dept. Industrial and Manufacturing Systems Engineering
University of Michigan Dearborn
Dearborn, USA
zhennhu@umich.edu

Abdallah Chehade
Dept. Industrial and Manufacturing Systems Engineering
University of Michigan Dearborn
Dearborn, USA
achehade@umich.edu

Christopher Pannier
Mechanical Engineering Department
University of Michigan Dearborn
Dearborn, USA
pannier@umich.edu

***Abstract*— Fused Filament Fabrication (FFF) is one of the most common additive manufacturing tools. With the aid of the open-source community, constant improvements in the mechanical build, electronic components, thermal design, and software algorithms allowed for increased reliability and part quality. However, issues persist in extrusion control, manifesting as deposition errors that degrade the visual and mechanical properties of the printed part. Current feedforward control techniques use a simplified model of the extrusion process as a first order system. However, such assumption fails to capture non-linear extrusion dynamics. Therefore, to build a controller that can improve quality under varied extrusion velocities, a more descriptive model is required. In this work, we introduce a cyber-physical system with industrial grade motion stages and controllers that can record feedback information from the drive motors of the 3D printer such as position, velocity, acceleration, and motor current. Additionally, a temperature sensor near the nozzle exit records the surface temperature of the nozzle. The printed geometry is scanned using a laser line profilometer. Using this system, single bead lines were printed with sinusoidally varying bead width. To create a model for extrusion dynamics, a nonlinear auto regressive exogenous (NARX) neural net is employed to predict the bead area given the extrusion velocity, tangent velocity, temperature, and motor current. The resulting trained NARX net provided predictions with low mean absolute error values between 0.0923 and 0.0994 using testing sets that are independent from training sets.**

***Keywords*— additive manufacturing, 3D printing, fused filament fabrication, narx net, cyber physical system**

I. Introduction

Additive manufacturing has a plethora of different methods that apply to polymeric, metallic, or ceramic materials. However, due to simplicity of operation and low feedstock cost, polymer fused filament fabrication has become the most common 3D printing method. A desktop example of a FFF 3D printer can be obtained for less than $200 as of 2023. Most FFF systems are a combination of a standard cartesian gantry with an extrusion system. Emerging FFF 3D printers such as the bambu labs X1 (Bambu lab, Shenzhen, China) and the Prusa MK4 (Prusa Research, Prague, Czech Republic) are cyber physical systems (CPS) as they combine and integrate computational algorithms and physical components in their operation. Current FFF 3D printing systems integrate internet of things (IoT) and connectivity features that allow for online monitoring, status feedback, and control. FFF 3D printers operate based on digital models that are modeled using computer aided design (CAD) tools. The CAD information is a cyber component that is translated into machine-readable code (gcode) that the physical system can processes. The physical component of the system involves the actual printing process where the model is created by stacking layers to create the 3D physical object. Additionally, sensors are used for real-time feedback and control of the printing systems thermal components. This dynamic interaction between the cyber and physical components makes FFF 3D printers a cyber physical system. Modern FFF 3D printers integrate a larger number of sensors, and a higher level of connectivity, further emphasizing the cyber-physical nature of FFF 3D printers.

The extrusion system in FFF 3D printers uses polymer thermoplastic filament. The filament is driven down the heater using an extrusion motor, where it is liquified, and the molten polymer is pushed through an orifice with a smaller diameter than the feed filament. An extruder cutaway is shown in Figure 1.

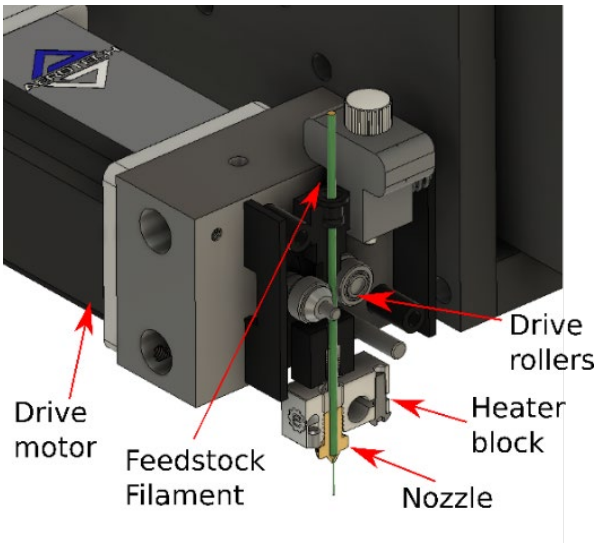

Fig. 1. A cut away of the extrusion system in the system of this paper

As the molten polymer is pushed through the nozzle, the carriage holding the extruder translates across the build plate. The relative velocity between the nozzle and the build plate leaves a bead with a pill-shaped cross section. Under steady-state condition, the cross-sectional area of the bead is proportional to the relative velocity of the extruder to the build plate.

Instrumentation of FFF 3D printing systems has been introduced in prior literature. Rossi et. all created an instrumented system FFF 3D printer using a low-cost desktop unit as a base, where they monitored the extrusion motor velocity, extrudate temperature, and extrusion force to verify a Nonlinear Autoregressive with eXogenous inputs (NARX) neural net model of extrusion force that was trained on physics-based simulation data [1]. Phan et al. used extrusion motor current feedback to estimate the general Nusselt number–Graetz number correlation to be used in rheological modeling [2]. Niehaus et al. used a force sensor to measure the extrusion force generated by different nozzle geometries to identify the most ideal parameters for the inner angles of the nozzle [3]. Moretti et al used a combination of a high-speed optical camera, force sensor, and an infrared thermal imaging to validate the simulation results [4].

Extrusion in FFF is a dynamic process, given a step input in extrusion velocity, the output velocity does not respond in a step-like fashion. Instead, the response is similar to a capacitor charging voltage over time, with some time constant. Additionally, the time constant for the extrusion velocity to reach the theoretical target velocity is not constant [5], making the use of standard linear modeling and control techniques difficult. The different time constant or dynamic response of the system is influenced by extrusion speed, nozzle geometry, standoff height, and extrudate temperature. These can be explained by the complex interaction between pressure, temperature, and viscosity. Where the viscosity of the melt is impacted by the temperature of the extrudate, the pressure is affected by viscosity, which in turn is affected by temperature. Therefore, the resulting dynamics are highly non-linear and difficult to model using a first principles approach.

Present control strategies for motion and extrusion control are open loop and feedforward in nature. These approaches fall short in accurately predicting and compensating for extrusion dynamics. Therefore, extrusion errors are a common occurrence, manifesting as under-extrusion at extrusion start-up and over-extrusion at extrusion halt as demonstrated in Figure 2.

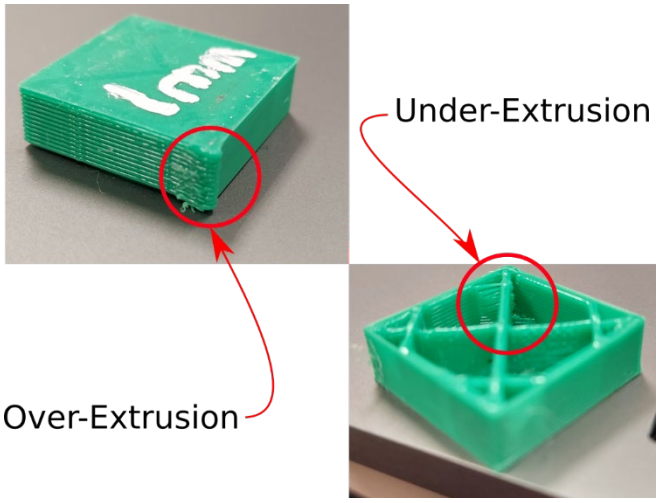

Fig. 2. Extrusion issues because of poor extrusion control resulting in over-extrusion extrusion or “blobs” at stops or under-extrusion causing missing features such as the missing infill section highlighted in the figure.

Data driven modeling techniques have become a common tool for modeling dynamic systems, they are preferred due to their quick computation and ease of construction. In FFF 3D printers, the response at any given time is the result of the state of the system at that point in time as well as a number of previous timesteps. Multiple data driven techniques can accept a time series input for modeling and prediction. The difficulty with data driven modeling techniques is the collection of a large number of high-quality datasets for training and testing. Therefore, there exists a need for a highly instrumented system with streamlined data collection and processing framework for collecting a large number of datasets for data driven modeling. This work describes the build of an industrial grade instrumented cyber physical FFF 3D printer with time synchronized position, velocity, current feedback as well as 3D surface scanning of printed geometry. The instrumented cyber physical system allowed for the easy collection of feedback signals and scans that were used to train a NARX-Net for bead area prediction using indirect sensors such as motor current sensor. These models allow for the future applications of modern control techniques of the FFF 3D printing systems to enhance printing accuracy and speed.

II. Instrumented FFF System

A. Gantry Components

To collect high quality datasets, high resolution, and high accuracy sensors are required. Therefore, retrofitting feedback

sensors on an existing desktop FFF 3D printer frame was considered unfeasible. The overall design is a cartesian based system with twin Z-Axis towers that carry the X-Axis stage, while the Y-Axis stage is directly bolted to the optical table. The Z-Axis installed were Aerotech Pro-115SL (Aerotech, Pittsburg, PA) linear stages with rotary motor and ball screw drive mechanisms. The X and Y stages are Aerotech Pro-165LM with linear motors for high speed and high acceleration. The extruder is driven by an Aerotech BMS35 motor coupled with a custom machined aluminum block to the E3D Hemera extruder with the E3D Revo nozzle with a diameter of 0.6 mm. The Z stages are mounted upright using WV3 angle bracket (Isel, Eichenzell, Germany). The X-Axis stage is mounted using two custom machined 25x50 mm extrusions. The mounting plates that couple the X-Axis extrusions to the Z-Axis stages were custom machined from 6 mm thick aluminum plates. The heated build plate was extracted from a Creality Ender-3 (Shenzhen Creality 3D Technology, Shenzhen, China) and rigidly mounted to the Y-Axis plate. The temperature at the tip was measured using a generic NTC100K thermistor. All the motors were driven using single axis Aerotech NDRIVE CP drives. The system components are summarized in Figure 3 and 4.

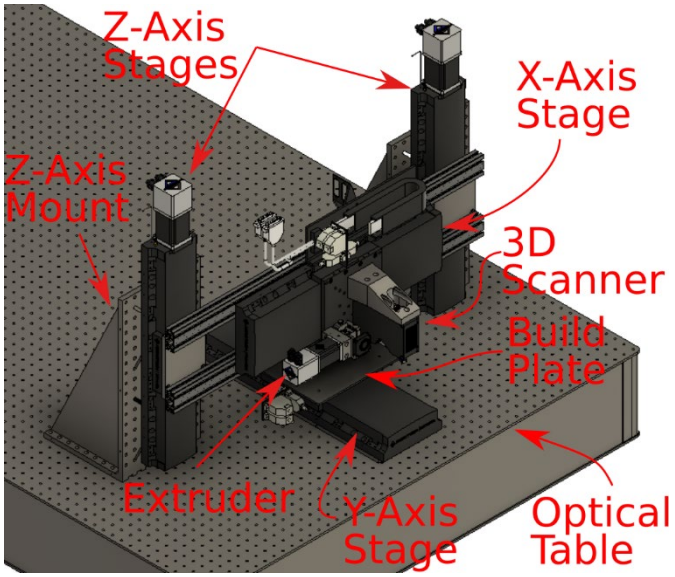

Fig. 3. Overview of instrumented system components

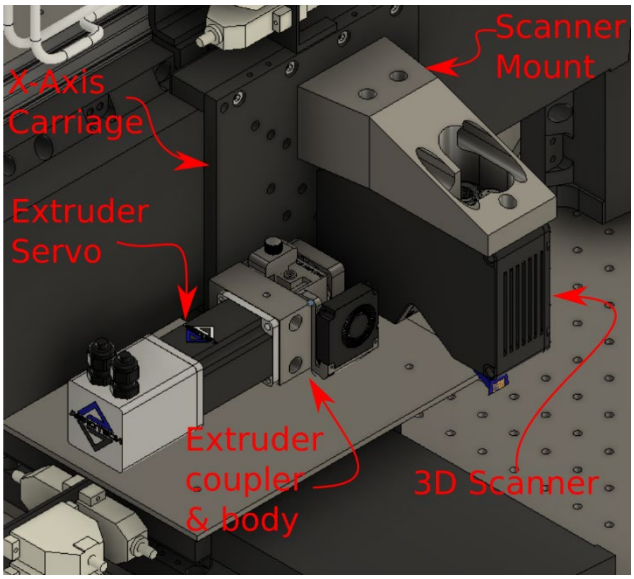

Fig. 4. Close up of the extrusion and scanning components.

B. *Sensor Components*

All the drive motors have position, velocity, acceleration, and current feedback with a sampling frequency of 1 KHz. The thermistor temperature values are measured using a voltage divider circuit and fed into the analog input of the Y-Axis drive. The Z-Axis stages encoders are capable of measuring position with a 2 µm linear resolution. The X and Y stage encoders are capable of measuring position with a resolution of 5 nm. The filament position can be measured with a resolution of 13 µm, however, this is not a direct measurement, as it is calculated from the diameter of the hobbed gear driving the filament. The printed bead area is scanned using a Gocator 2410 laser line profilometer (LMI Technologies, Vancouver, Canada) with a line resolution of 5 µm and a line spacing of 70 µm. A sample of a scan is shown in Figure 5.

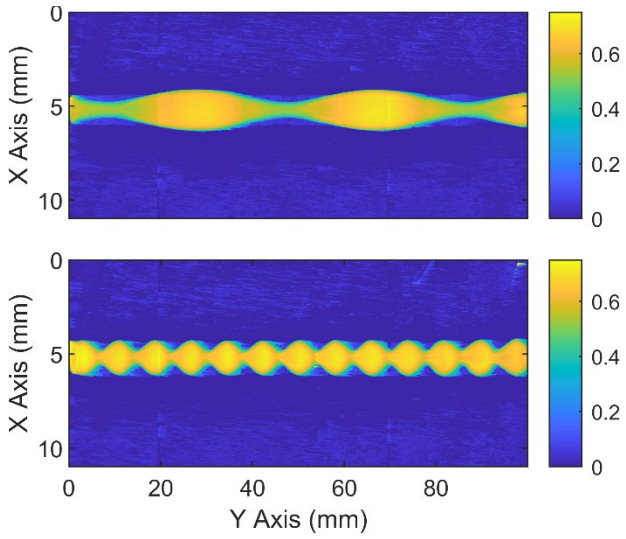

Fig. 5. Leveled scans of printed beads with varying periods.

C. Data Analysis Framework

For each experiment, a single straight bead was printed with a sinusoidally varying bead width to excite the dynamics of the system. The values of the sine wave period and amplitude were varied across the experiments. During each experiment, the experiment time, Y axis position, Y axis velocity, E axis velocity, E axis current, and thermistor readings were recorded at 1 KHz using the Aerotech A3200 Digital Scope software and then exported as ".mat" files. After printing, the bead is scanned, and the 3D surface scan is exported as a ".csv" file. Each experiment data is then fed into MATLAB for analysis. The csv file that is outputted from the scanner is a series of line profiles along the bead that combine to a complete surface of the bead. The build plate upon which the bead is printed is not flat. Therefore, a flattening algorithm is used to flatten the scan prior to numerically integrating the area underneath each scan line to calculate the area. The output scans can contain missing values for some of the pixels, which are filled using the average values of the 8 surrounding pixels.

III. NARX-Net Implementation

A. Experiment Design

As mentioned prior, the bead area is a function of the ratio between the extrusion velocity and the tangent velocity of the print head. The bead area and its components are related using the following formula that is extracted using the continuity condition:

$$A_B = \frac{V_e A_f}{V_y} \quad (1)$$

where A_B is the bead Area, V_e is the extrusion velocity, A_f is the cross-sectional area of the filament used, V_y is the velocity of the extruder head. We use subscript y as we actuate along the Y-Axis only.

From the prior relation, it can be observed that the bead area could be varied by either, 1) holding V_e constant while varying V_y, or 2) by holding V_y constant while varying V_e. The printing conditions are summarized in Figure 6.

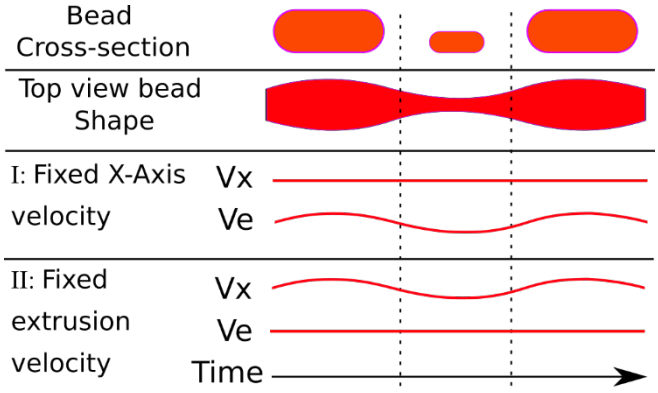

Fig. 6. The two conditions used in generation of the bead area signal used for driving the extruder or Y-Axis.

The first condition is more conducive to observing the spreading dynamics of the bead while the second condition mainly observes the dynamics of the extruder itself. We divided our experiments roughly equally between both conditions.

In each experiment, a single bead is printed with a sinusoidally varying bead width. The printing speed and period of the bead area was varied between values that were found to be the physical limits by trial and error. The distribution of the values for the printing speed and bead area width were calculated using a Latin hypercube design. The values of the sine wave period varied between 5 mm and 50 mm, while the values of the extrusion velocity were varied between 1- 4 mm/s for fixed extrusion velocity condition. For the fixed Y-Axis velocity, the velocity was varied in the range of 10-25 mm/s. These values result in bead widths that vary from 0.75-3.00 mm with a fixed 0.3 mm layer height.

The bead signal area is translated into position time (PT) commands using a MATLAB script for the Y-Axis and extrusion axis, this format is fed into the Aerotech motion composer application as an aerobasic program. The PT commands allow for accurate control of the position within a specified time. In each experiment the commands were sent into the Aerotech motor drivers at a frequency of 1 KHz. A sample of the input format is shown in Figure 7.

```
PT Y15 A5 TIME 1
PT Y15 A5.004 TIME 1
PT Y15 A5.008 TIME 1
PT Y15 A5.012 TIME 1
PT Y15.0013 A5.016 TIME 1
PT Y15.0144 A5.02 TIME 1
```

Fig. 7. The command style for position of the Y-Axis as well as the A-Axis (extruder), the commands are executed with the specified time value of 1 millisecond.

B. NARX-Net training and testing

1) NARX-Net

A NARX neural network is an artificial neural network that models and predicts time series data. Its ability to model and predict time series data allows it to capture temporal dependencies by incorporating auto regressive elements, additionally, it can account for external factors by incorporating exogenous inputs. These features make it well suited to our application of system identification and modeling of the extrusion system. The mathematical expression of the NARX-Net used in this work is described in equation 2. The network diagram is shown in Figure 8.

$$y(t+k) = f\left(\sum_{i=1}^{10} W_{oi}.\sigma\left(\sum_{j=0}^{10} W_{ij}.u(t-j) + W_{hl}.y(t-30) + b_i\right) + b_o\right) \quad (2)$$

where $y(t+k)$ is the predicted output at time $t+k$. $f(.)$ is the activation function. W_{oi} are the hidden weights from the hidden neurons to the output. $\sigma(\cdot)$ is the activation function that is applied to the weighted sum of the inputs. W_{ij} are the weights from the input u to the hidden neurons. $u(t-j)$ is the time delayed input, W_{hl} are the weights from the output y to the hidden neurons. $y(t-30)$ is the time delayed output, and b_i,

b_o are the bias values for the hidden layer and output layer, respectively.

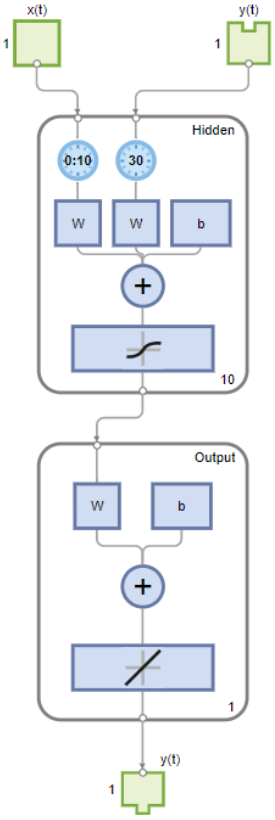

Fig. 8. Design of the NARX-Net used for training on the experimental feedback data, where W stands for the network weights, b stands for the network biases. The hidden layers are shown to have "tansig" activation functions while the output layer is shown to have a linear activation function.

The inputs selected for training of the NARX-Net were time series of extrusion servo velocity, Y-Axis velocity, nozzles temperature, and extrusion servo current. The output was a time series of the measured bead area. The NARX-Net was built using 10 neurons with the prior 10 time steps used for the input, and 30th time step for the output. The NARX-Net was trained in an open loop mode, where the observed output from the previous timesteps is used for prediction of the future timesteps.

The NARX-Net was trained under two conditions,1) using the inputs of Y-Axis velocity, extrusion velocity, temperature, and extruder motor current and the output of bead area, 2) using the inputs of Y-Axis velocity, extrusion velocity, temperature and the output of the extruder motor current. Condition 2 is a more suitable model for open loop implementation, as motor current values are fed-back in real time. While scanning is not a real time feedback mechanism due to physical constraints.

To evaluate the performance of the NARX-Net, a subset of the experiments was set aside as a testing set. Out of the 39 experiments, 30 experiments were used for training while 9 were used for testing and validation. The performance of the NARX-Net was evaluated using residual standard error (RSE) with equation 3.

$$RSE = \sqrt{\frac{1}{n-2}\sum_{i=1}^{n}(y_i - \hat{y}_i)^2} \quad (3)$$

And the coefficient of determination, as per equation 4.

$$R^2 = \frac{\sum_{i=1}^{n}(y_i - \bar{y}_i)^2}{\sum_{i=1}^{n}(y_i - \bar{y})^2} \quad (4)$$

As well as the mean absolute error (MAE), as per equation 5.

$$MAE = \frac{\sum_{i=1}^{n}|y_i - \bar{y}_i|^2}{n} \quad (5)$$

Where y_i is the ith testing set output and $\hat{y}_i$ is the corresponding NARX-Net predicted output.

IV. Results

For condition 1, the bead area predictions show low values of MAE. The same low values of MAE are shared for the training and testing sets. Figure 9 & 10 show the predictions vs. observations for the training and testing sets, respectively.

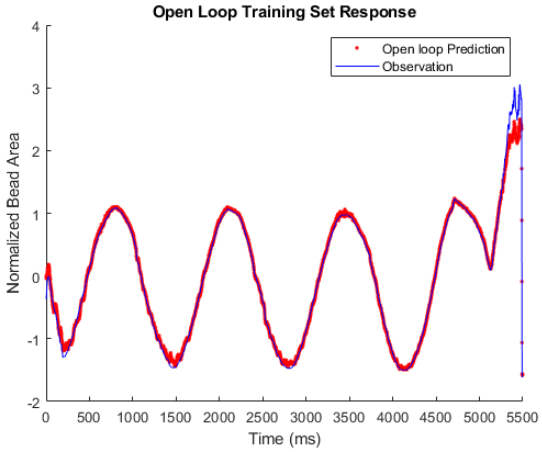

Fig. 9. Bead area response of the training dataset using the trained NARX-Net.

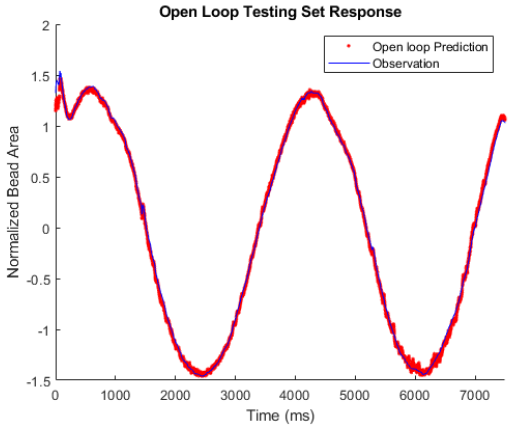

Fig. 10. Bead area response of the testing dataset using the trained NARX-Net.

The performance of the NARX-Net for the first condition is summarized in Table 1.

TABLE. 1. Performance metrics for the bead area predictions of the NARX-Net.

Metric	Training Set	Testing Set
	Open-Loop	
RSE	0.1977	0.1858
R^2	0.9608	0.9652
MAE	0.0994	0.0930

Using Condition 2, a similar performance to condition 1 is observed. Figure 11 & 12 show the predictions vs. observations for the training and testing sets, respectively.

Fig. 11. Extrusion motor current prediction of the training dataset using the trained NARX-Net.

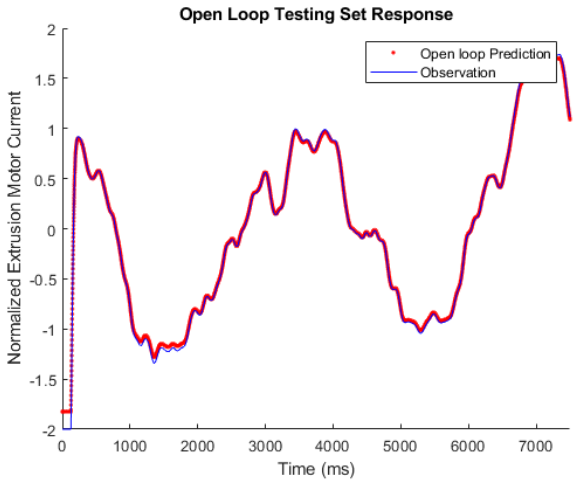

Fig. 12. Extrusion motor current prediction of the testing dataset using the trained NARX Net.

The performance of the NARX-Net for the second condition is summarized in Table 1.

TABLE 2. Performance metrics for the motor current predictions of the NARX-Net.

Metric	**Training Set**	**Testing Set**
	Open-Loop	
RSE	0.1819	0.1706
R^2	0.9439	0.9475
MAE	0.0984	0.0923

V. Disscussion and Conclusion

The aim of this paper was to introduce an instrumented FFF 3D printing system with high resolution feedback. The system's goal is to serve as a data collection platform with the aim of building data driven models and testing of modern control algorithms for FFF systems.

In this work, the system was used to collect time synchronized data sets that were later used to build a rudimentary data driven model using NARX-Net. The NARX-Net models provided high accuracy predictions in open loop setup. Under the second condition, an open loop format can be used as a practical model of the system, as the extrusion motor current feedback is available as an "online" signal.

The system's performance can be further improved with the following planned enhancements. A faster response of the molten flow temperature can be obtained by placing a thermocouple to be in contact with the flow. Additionally, the number and size of the training data set can be increased for better closed loop predictions.

VI. Acknowledgements

This research was supported by the U.S. Department of Defense under Cooperative Agreement Award No. HQ0034-20-2-0007.

References

[1] A. Rossi, M. Moretti, and N. Senin, "Neural networks and narxs to replicate extrusion simulation in digital twins for fused filament fabrication," *Journal of Manufacturing Processes*, vol. 84, pp. 64–76, 2022. doi:10.1016/j.jmapro.2022.09.048

[2] D. D. Phan, Z. R. Swain, and M. E. Mackay, "Rheological and heat transfer effects in fused filament fabrication," *Journal of Rheology*, vol. 62, no. 5, pp. 1097–1107, 2018. doi:10.1122/1.5022982

[3] V. Nienhaus, K. Smith, D. Spiehl, and E. Dörsam, "Investigations on nozzle geometry in fused filament fabrication," *Additive Manufacturing*, vol. 28, pp. 711–718, 2019. doi:10.1016/j.addma.2019.06.019

[4] M. Moretti, A. Rossi, and N. Senin, "In-process simulation of the extrusion to support optimisation and real-time monitoring in fused filament fabrication," *Additive Manufacturing*, vol. 38, p. 101817, 2021. doi:10.1016/j.addma.2020.101817

[5] O. Habbal, A. Kassab, G. Ayoub, P. Mohanty, and C. Pannier "System Identification of Fused Filament Fabrication Additive Manufacturing Extrusion and Spreading Dynamics" *Solid Freeform Fabrication Conference proceedings,* 2023